Journal of Functional Foods 116 (2024) 106180

Contents lists available at ScienceDirect

Journal of Functional Foods

journal homepage: www.elsevier.com/locate/jff

Rosemary essential oil microemulsion prevents DSS-induced intestinal injury in mice by modulating IL-17 signaling pathway

Jie Wang [a,c,1], Yanzhuo Jia [b,1], Ning Xia [a,c,1], Xuan Wang [a,c], Peijie Zhou [a,c], Jiawei Duan [a,c], Jinkai Li [a,c], Taotao Li [a,c], Tiantian Tang [a,c], Yujiao Wang [a,c], Ding Liu [a,c], Huanxian Shi [a], Yundong Xie [a], Chongbo Zhao [a,c], Jing Sun [a,c,*], Xiaofei Zhang [a,c,*]

[a] Key Laboratory of Basic and New Drug Research in Chinese Medicine, Shaanxi University of Chinese Medicine, Xianyang, Shaanxi 712046, China
[b] Chang'an Road Community Health Center, Beilin District, Xi'an, Shaanxi, 710000, China
[c] Shaanxi Provincial University Engineering Research Center of Chinese Medicine Aromatic Industry, Shaanxi University of Chinese Medicine, Xianyang, Shaanxi 712046

ARTICLE INFO

Keywords:
Rosemary essential oil microemulsion
Ulcerative colitis
Mechanisms of action
Transcriptomics
IL-17 signaling pathway

ABSTRACT

Rosemary (*Rosmarinus officinalis* L) is a medicinal and edible plant. Rosemary essential oil (REO) is the principal constituent of rosemary and possesses anti-inflammatory and antioxidant properties. In this study, we evaluated the cell viability and anti-inflammatory activity of REO through the MTT assay and LPS-induced NO production in mouse RAW264.7 cells, respectively. The optimal formulation for the preparation of REO- microemulsion (REO-ME) was determined employing reversed-phase emulsification in conjunction with pseudo-triphasic diagrams. Transcriptomics, combined with network pharmacology, was employed to identify key signaling pathways, and molecular docking analysis was performed to investigate the relationship between the active ingredients of REO-ME and the key targets. The results showed that REO-ME is an O/W type ME. In addition, further pharmacodynamic experiments showed that REO-ME inhibits the expression of inflammatory factors such as IL-6, IL-1β, and TNF-α by regulating the key targets in the IL-17 signaling pathway, thereby to alleviating UC.

1. Introduction

Ulcerative colitis (UC) is a distinct colonic mucosal disorder, representing one facet of inflammatory bowel disease (IBD), with clinical manifestations of abdominal pain, diarrhea, and blood in the stool (Zhu et al., 2021). It is characterized by its propensity for recurrence, prolonged disease duration, and challenges in achieving remission (Wang et al., 2021a). In recent years, there has been a gradual escalation in the prevalence and incidence of UC, imposing a substantial burden on global healthcare systems and economies (Wu, 2022). The pathogenesis of UC is complex, involving factors such as genetic predisposition, epithelial barrier disruptions, dysregulated immune responses, neutrophil infiltration, and pro-inflammatory cytokines (Ordás et al., 2012; Shalaby et al., 2023). Currently, the primary therapeutic options for patients with mild to moderate UC encompass glucocorticoids, 5-aminosalicylic acid, immunosuppressants, and corticosteroids. However, the utilization of these medications is associated with a range of challenging side effects, such as susceptibility to relapse, hypertension, and cardiac complications (Zhang et al., 2022b). In cases of intractable diseases or colon tumors, etc., the removal of the colon is necessary for treatment, which can effectively alleviate the pain of the patients; however, it significantly impairs their quality of life (Caprilli et al., 2007; Noviello et al., 2021; Ordás et al., 2012). Therefore, the limitations of existing drugs and the shortcomings of surgery underscore the pressing need to explore novel approaches for UC treatment.

Interleukin (IL)-17 is a marker inflammatory factor associated with

Abbreviations: UC, Ulcerative colitis; IBD, inflammatory bowel disease; IL-17, interleukin-17; IL-6, interleukin-6; NF-κB, nuclear factor kappa-B; IL-1β, interleukin-1 beta; TNF-α, tumor necrosis factor-α; DSS, Dextran Sodium Sulfate; SDS-PAGE, Sodium dodecyl sulphate–polyacrylamide gel electrophoresis; ME, Microemulsion; REO, Rosemary essential oil; RNA-seq, RNA sequencing; REO-ME, Rosemary Essential Oil Microemulsion; ELISA, Enzyme-linked immunosorbent assay; WB, Western blot; PVDF, polyvinylidenefluoride; TBST, tris buffered saline Tween; ECL, Electrochemiluminescence; GO, gene Ontology; KEGG, Kyoto Encyclopedia of Genes and Genomes; WGCNA, Weighted gene co-expression network analysis; GEO, Gene Expression Omnibus.

* Corresponding authors.
E-mail addresses: ph.175@163.com (J. Sun), 2051028@sntcm.edu.cn (X. Zhang).
[1] These authors contributed equally to this work and share first authorship.

https://doi.org/10.1016/j.jff.2024.106180
Received 4 February 2024; Received in revised form 29 March 2024; Accepted 9 April 2024
Available online 24 April 2024

Th17 cells that promotes the release of inflammatory factors Inflammation is inextricably linked to the development of UC (Fletcher et al., 2020; Ma et al., 2017; Wei et al., 2014). IL-17A has been implicated in the pathogenesis of inflammatory diseases and mediates inflammation by inducing neutrophils and chemokines (Wang et al., 2024a). Furthermore, IL-6 and IL-1β assume significant roles in inflammation by regulating immune responses and inflammatory processes (Li et al., 2022). Some drugs have been shown to exert therapeutic effects by inhibiting key targets of the IL-17 signaling pathway (Gao et al., 2022). Therefore, inhibiting the expression inflammatory factors associated with IL-17 signaling may represent an effective approach for treating UC.

Rosemary (*Rosmarinus officinalis* L.) is an aromatic plant belonging to the Labiatae family and exhibits a distinctive fragrance. It is native to temperate countries of the Mediterranean region and is presently cultivated worldwide (Grace et al., 2021; Li et al., 2023). As a medicinal plant (Yan et al., 2022), rosemary is safe and non-toxic and has gained extensive utilization in the food industry as a food preservative and a flavoring agent for beverages (Romo Vaquero et al., 2012). In traditional medicine, rosemary has been employed to alleviate headaches, inflammation, and stomach pain (Fareed et al., 2023). Brindisi et al. found that rosemary extract exerts its anti-inflammatory effects by inhibiting the translocation of nuclear factor (NF)-κB to the nucleus (Brindisi et al., 2020). Rosemary essential oil (REO) represents the volatile substance of rosemary and possesses anti-inflammatory, analgesic, and antioxidant properties (Pelvan et al., 2022). Several studies have elucidated its anti-inflammatory potential. Oral administration of REO in rats has been shown to treat peritonitis and paw edema induced by carrageenan gum by reducing the extent of leukocyte migration and inflammatory exudate (Takaki et al., 2008). Eucalyptol and α-pinene, the primary components of REO, can regulate the inflammatory response by inhibiting the expression of IL-1β and NF-κB. Medicherla et al. (2016) found that REO treats UC by downregulating the expression of IL-6. However, the components and mechanisms underlying its therapeutic effects remain to be elucidated.

Essential oils, being natural extracts, find application in many fields. However, their bioactivity is susceptible to degradation upon exposure to light and they are also irritating and allergenic (Jampilek & Kralova, 2022), significantly restricting their utility. Microemulsions (ME), novel drug carriers, a thermodynamically stabilized system consisting of aqueous and oil phases along with emulsifiers and co-emulsifiers in appropriate proportions (Moghassemi et al., 2022), are characterized by their low viscosity, ease of preparation, small droplet size, high solubility, and favorable stability. ME have been found to enhance the utilization of essential oils, improve the solubility and stability of drugs, and are widely used in pharmaceuticals, cosmetics, food, and other fields (Ding et al., 2009; Shi et al., 2022). Currently, microemulsion-based drug delivery systems are a promising therapy for the treatment of intestinal inflammatory diseases (Vitória Minzoni de Souza Iacia et al., 2024). Therefore, we investigated the mechanism of action on UC by formulating REO into a Rosemary Essential Oil Microemulsion (REO-ME).

RNA sequencing (RNA-seq) is a high-throughput DNA assay that enables the investigation of gene function and structure at a holistic level (Wang et al., 2021b). It is employed for differential gene expression analysis (Wang et al., 2024b). Weighted gene co-expression network analysis (WGCNA) is an analytical method based on RNA-seq analysis, clustering genes with similar expression patterns, elucidating associations between modules, specific genes, and traits, and assessing gene expression across multiple samples. It is now widely used to gain biological insights into multiple diseases and conduct association analyses between traits and genes (Zhang et al., 2022a). Network pharmacology leverages computer software technology and network databases to predict drug-disease target interactions, constructing relationship network diagrams that unveil drug-disease associations involving multiple targets and pathways at various levels (Hao et al., 2021). Nevertheless, Network Pharmacology soely analyzes the relationship between a drug and a disease, neglecting the impact of drug components on the outcome. This oversight can lead to predictions of mechanisms that may differ from reality. In this study, oral bioavailability (OB) and the relative content of each REO component were employed as key parameters. Additionally, the novel algorithm "weighting factor" algorithm (Wang et al., 2023) was employed to reanalyze Gene Ontology (GO) and Kyoto Encyclopedia of Genes and Genomes (KEGG) date to identify key signaling pathways, and enhance the reliability of the obtained results.

In this study, was aimed to formulate a ME containing REO (REO-ME) and investigate its mechanism of action upon oral administration in a dextran sodium sulfate (DSS)-induced UC murine model. Initially, the anti-inflammatory effects of REO were analyzed in conjunction with in vitro experiment. Subsequently, the optimal ME formulation was determined using pseudo-ternary phase diagrams. The therapeutic efficacy of REO-ME was evaluated through animal experiments, while potential signaling pathways of action were elucidated using network pharmacology. To further validate the therapeutic potential of REO-ME for UC, we conducted transcriptome sequencing, enzyme-linked immunosorbent assay (ELISA), WGCNA, immunohistochemistry, and western blot (WB). Our findings provide novel research avenues for the treatment of UC using REO-ME.

2. Materials and methods

2.1. Experimental materials

An MTT kit was obtained from Shanghai Yuchun Biotechnology Co., Ltd.; while a nitric oxide (NO) kit was sourced from Nanjing Jiancheng Bioengineering Institute (Catalog No. A012-2–1). IL-17, IL-6, TNF-α, and IL-1β kits were procured from Jiangsu Meimian Industrial Co., Ltd.

2.2. Extraction and compositional analysis of REO

Rosemary (*R. officinalis* L.) was purchased from Yuzhou Senmao Rosemary Biotechnology Co. Fresh herbs were cultivated in Yuzhou City, Henan Province (33°59′-34°24′ N, 113°03′-113°39 ′E) (Li et al., 2012). Subsequently, the herbs were dried post-harvest for subsequent experimentation. Prof. Hu Benxiang of Shaanxi University of Chinese Medicine authenticated the rosemary herb. REO was extracted through water vapor distillation. Initially, 100 g of dried rosemary was placed in a round-bottomed flask containing 1200 mL of distilled water and refluxed for 2 h to obtain REO (Akhbari et al., 2018; Li et al., 2024). The obtained REO was dehydrated with anhydrous sodium sulfate, and its composition was determined using GC–MS. The chromatographic conditions included the following: an Agilent HP-5MS column (30 m × 250 μm × 0.25 μm), high-purity helium as the carrier gas, an inlet temperature of 270 °C, an injection volume of 1.5 μL, and a flow rate of 1 mL/min with a split ratio of 30:1. The column temperature was initially set at 50 °C and was then increased to 71 °C at a rate of 3 °C/min, and further increased to 91 °C at 20 °C/min, reaching 140 °C at 3 °C/min, and finally maintained at 250 °C at 20 °C/min for 1 min. Mass spectrometry conditions were as follows: the electron impact (EI) ion source temperature of 230 °C, the MS quadrupole temperature of 150 °C, a solvent delay time of 2 min, and a mass scanning mode of full scanning within a range of 30–550 amu.

2.3. Characterization of REO chemical composition

REO data were processed using DataAnalysis and analyzed against a standard solution of n-alkanes (C8-C40). The retention index (RI) of the components were calculated using Equation (1), Subsequently, the results were employed in conjunction with the NIST Standards Library to ascertain the composition of the REO.

$$RI = 100n + 100[t_R(x) - t_R(w)]/t_R(w+1) - t_R(w) \quad (1)$$

In Equation (1), "n" represents the number of carbon atoms in n-alkane hydrogens preceding the peak of REO, "t_R (x)" denotes the retention time of REO, "t_R (w)" signifies the retention time of n-alkane hydrogens preceding the REO peak, and "t_R (w + 1)" represents the retention time of n-alkane hydrogens following the REO peak. Additionally, it was considered that t_R (w) < t_R (x) < t_R (w + 1).

2.4. In vitro experiments

2.4.1. Cell culture

RAW264.7 cells were purchased from Wuhan Pu Nosai Technology Co. and cultured in Dulbecco'-s Modified Eagle'-s Medium (DMEM) supplemented with 10 % fetal bovine serum and 1 % penicillin–streptomycin. These cells were incubated in a 5 % CO_2 atmosphere at 37 °C.

2.4.2. Determination of cell viability via MTT assay

Cell viability was determined using the MTT assay. RAW264.7 cells (100 μL of cell suspension) were seeded in 96-well plates and incubated at 37 °C for 24 h. For the MTT assay, cells were exposed to various concentrations of REO and REO-ME (0.5, 1.0, and 2.0 μg/mL) for 24 h. Control ME was used as a negative control and administered according to the concentration of REO-ME. Subsequently, 10 μL of MTT solution was added to each well, followed by further incubation at 37 °C for 4 h. After incubation, the supernatant was removed, and 110 μL of formazan lysis solution was added, with agitation for 10 min. The optical density (OD) value was then measured at 490 nm to calculate cell viability and determine the optimal concentration of REO and REO-ME. The calculation formula used was as follows:

$$Cellviability = (OD\bar{x}_S - OD\bar{x}_K)/(OD\bar{x}_C - OD\bar{x}_K) \times 100\% \quad (2)$$

In Equation. (2), "$OD\bar{x}_S$" "denotes the OD value of the measuring wells;" "$OD\bar{x}$" "denotes the OD value of the blank well; and" "$OD\bar{x}_C$" "denotes the OD values of the control wells".

2.4.3. Effect of REO on the levels of NO released by LPS stimulated RAW264.7 cells

NO, a vascular endothelial diastolic factor, is a highly reactive free radical in biological systems and plays a pivotal role in inflammatory responses (Ma et al., 2010). In this study, we assessed the anti-inflammatory potential of REO by using a model of LPS-induced cellular inflammation. A 100 μL aliquot of cellular suspension (2×10^6/mL) was dispensed into each well of 96-well plates, followed by overnight incubation at 37 °C in a 5 % CO_2 incubator. Subsequently, 90 μL of REO at various concentrations (0.5, 0.7 and 0.9 μg/mL), determined through the MTT assay for cell viability, were added to each well. After a 4 h incubation period, an LPS solution (1.0 μg/mL) (Park et al., 2022) was introduced into each well, and the cells were incubated overnight to establish an inflammation model. Absorbance values were measured at 550 nm following the instructions provided with the NO kit.

The following formula was used for the calculation:

$$NOcontent(\mu mol/L) = A_S - A_K/A_B - A_K \times C_B \times N \quad (3)$$

In Equation. (3), "A_S" "denotes the OD value of assay wells;" "A_K" "represents the OD value of blank wells;" "A_B" "denotes the OD value of standard wells;" "C_B" "denotes the concentration of the standard (20 μmol/L); and "N" denotes four-fold dilution.

2.5. Preparation of REO-ME

2.5.1. Screening for optimal REO-ME preparation

In this experiment, we constructed pseudo-ternary phase diagrams by titrating water to determine the prescription of REO-ME (Seok et al., 2018), using 5 g. of prescription. REO-ME was prepared by mixing the isopropyl myristate (IPM) and REO at a 1:1 ratio as the oil phase, followed by the addition of surfactant and co-surfactant at varying mass ratios (9:1, 8:2, 7:3, 6:4, 5:5, 4:6, 3:7, 2:8, and 1:9). The quantity of aqueous phase added during the preparation process was recorded, and the mass percentages for the oil phase, aqueous phase, surfactant, and co-surfactant in the system were calculated. The optimal ratios of surfactant, co-surfactant, and oil phase, as well as temperature and surfactant/co-surfactant (KM) values, were ascertained.

2.5.2. Characterization of REO-ME

REO-ME was contained in a bottle, and its clarity and flowability were observed. A copper mesh, which contained a Formvar support film, was positioned on the sealing film. Approximately 10 μL of REO-ME was then added dropwise on to the carbon film, allowing it to hold for 20 s, following which any excess sample was carefully removed using filter paper. Phosphotungstic acid (20 mg/mL) was prepared, with the pH was adjusted to approximately 7 using NaOH. This solution was subsequently filtered through a 0.22 μm organic filtration membrane before being added dropwise onto the copper mesh. Each application of the staining solution was allowed to discolor for 20 s, with this procedure repeated three times. Any excess staining solution was absorbed using filter paper, and the sample was then dried. Thereafter, the morphology of the sample was observed using a lanthanum hexaboride projection electron microscope (Nihon Electronics JEM-2100Plus). Two separate REO-ME samples of equal volumes were mixed with two dyes: Sudan III, which is oil-soluble, and methylene blue, which is water-soluble. According to the principle of similarity and dissolution, when the rate of red diffusion exceeded that of blue, the emulsion was classified as W/O; conversely, when the rate of blue diffusion exceeded that of red, it was categorized as O/W. Furthermore, 1 mL of REO-ME was diluted with pure water, and subsequently, the particle size and Zeta potential were measured using a particle size meter (ZEN3600, Malvern Instruments Ltd.).

2.6. Comparison of REO and REO-ME pharmacodynamics

2.6.1. Animal grouping and the establishment of an UC model

Forty Specific pathogen-free (SPF) BALB/c male mice were purchased from Chengdu Dashuo Laboratory Animal Co. Ltd. in China (Animal License: SYXK [Chuan] 2019–189). All study procedures adhered to the guidelines set forth by the Ethics Committee of Shaanxi University of Chinese Medicine (Ethics No.: SUCMDC20210520001). Following a 7-day feeding acclimatization period, the mice were randomly divided into control, model, positive drug, REO, and REO-ME groups. Except for the control group, all other groups were free to drink a 3 % dextran sodium sulfate (DSS) solution for modeling purposes. Administration of REO (250 mg/kg), REO-ME (250 mg/kg) calculated from the amount of REO in the REO-ME, and the positive drug (mesalazine) commenced on the second day of modeling and continued for 10 consecutive days. During the experimental period, the mice were assessed using disease activity index (DAI) scores, which involved monitoring changes in body weight, fecal characteristics, and the presence of blood in stool. The DAI was calculated as (changes in body weight + fecal characteristics + blood in stool)/3 (Wang et al., 2021c).

2.6.2. Sample collection

Blood was obtained from the eyes of mice 4 h after administration. The blood samples were subsequently centrifuged, and the resultant supernatant was collected and stored by freezing. After euthanasia, mouse Colon were collected. The colons were then purged in saline, and then fixed, and preserved using 4 % paraformaldehyde.

2.6.3. Hematoxylin-eosin (HE) staining of colon tissue

Colon tissues from each group were fixed in 4 % paraformaldehyde. Subsequently, residual fixative and impurities were removed through rinsing with flowing water. The tissues were then dehydrated using an

ethanol gradient method, followed by xylene transparency treatment, wax embedding, sectioning, deparaffinization, and staining. photographing under the microscope for colon pathology assessment.

2.6.4. Determination of TNF-α and IL-6 expression in mouse serum by ELISA

According to the ELISA kit instructions, the absorbance values of each well were measured at a wavelength of 450 nm. Subsequently, a standard curve was constructed, and the concentrations of the inflammatory factors TNF-α and IL-6 in serum were calculated.

2.7. Network pharmacology

2.7.1. Construction of a "REO component-UC-key target" network map

PubChem (https://pubchem.ncbi.nlm.nih.gov/) and SwissTarget Prediction (https://www.swisstargetprediction.ch) databases were employed to predict targets associated with REO components. The search term "ulcerative colitis" was used to retrieve disease targets from DisGeNET (https://www.disgenet.org), Genecards (https://www.genecards.org), and OMIM (https://omim.org). The Gene Expression Omnibus (GEO) database was selected as the data source, with the GSE87466 dataset chosen for our study. Differential genes were identified using the limma package in R (Lu et al., 2021) (https://bioconductor.org/packages/release/bioc/ht-ml/limma.html), applying criteria set at $|\log FC| \geq 1$ and $p < 0.05$. The online software Venny 2.1.0 (https://bioinfogp.cnb.csic.es/tools/venny/index.html) was used to identify the intersecting genes among GEO differential genes, UC, and REO components. These intersecting genes were imported into Cytoscape 3.7.2 software and analyzed using the network analyzer tool, sorted by degree value. GO and KEGG enrichment analysis of the intersecting targets was performed using the R language and the enrichment results were reordered by introducing weight coefficients.

2.7.2. Determination of weighting factors

Traditional network pharmacology often overlooks the relative content of each component, thereby impacting experimental outcomes. Weighting coefficients play a crucial role in elucidating the significance of active ingredients and their relative proportions in experiments. OB serves as a pivotal parameter in drug metabolism in the body. The methodology employed in this study aligns with that established in a prior laboratory work (Wang et al., 2021c). The OB value of a constituent was associated with its respective weighting factor, as follows:

$$W = m \times b(OB) \tag{4}$$

$$T = \sum_{i=1}^{n} \mathrm{W}i \tag{5}$$

$$P = \sum_{i=1}^{n} \mathrm{T}i \tag{6}$$

In Equation (4), "W" denotes the weight coefficient assigned to each component, "m" signifies the relative content of individual components, and "b(OB)" represents the OB of these components, reflecting their proportions within the body following oral administration. As shown in Equation (5), where "T" denotes the weight coefficient of the target. Equation (6) then introduces "P" as the weight coefficient of the pathway.

2.8. Molecular docking

Utilizing the enriched targets in the pathway, the 3D structures of the heat shock proteins HSP90AA1, IKBKB, and RELA target proteins were downloaded in pdb format from the RSCB PDB, while the 2D structures of the components and characterized ligands were downloaded in sdf format from the PubChem database. Subsequently, molecular docking was performed using the LibDock tool within the Discovery Studio 4.0 software.

2.9. REO-ME pharmacodynamics

2.9.1. Experimental animals

To further evaluate the pharmacodynamics of REO-ME, we purchased 60 male SPF BALB/c mice from Chengdu Dashuo Laboratory Animal Co. in China. Following a 7-day acclimatization period, we randomly divided the mice into six groups: the control group, the model group, the positive drug group (mesalazine), and the REO-ME groups receiving low-dose (125 mg/kg), medium-dose (250 mg/kg), and high-dose (500 mg/kg) treatments (Takaki et al., 2008). Except for the control group, all other groups were induced with a 3 % DSS solution ad libitum for the purpose of modeling, and drug administration commenced on the second day of modeling, continuing for 10 consecutive days. The DAI scores were determined for each mouse. All animal experiments conducted were approved by the Ethics Committee of Shaanxi University of Chinese Medicine. Following the final administration, blood samples were collected from the eyeballs of mice in each group, centrifuged, and the resulting serum was stored at −80 ℃. Subsequently, after euthanasia, the colon was dissected and with saline. Subsequently, its length was measured, recorded, and divided into two segments for future use.

2.9.2. ELISA for assessment of inflammatory factors in mouse serum

The levels of inflammatory factors TNF-α, IL-6, IL-17, and IL-1β in mouse serum were performed according to the ELISA kit instructions, and the absorbance values of each well were measured at 450 nm.

2.10. Mouse RNA-seq analysis

Total RNA was extracted from the colon using Trizol lysate, followed by mRNA enrichment and reverse transcription into double-stranded cDNA. Subsequently, the double ends of the cDNA, along with the joints, were repaired, and an online library was constructed through PCR amplification. The library construction and sequencing processes were conducted by Jidiao Biotech Ltd. The RNA-seq data were subjected to bioinformatic analysis using Omicsmart (https://www.omicsmart.com), a real-time interactive online data analysis platform. Screening criteria for GO and KEGG pathway enrichment analysis included a significance level of $p < 0.05$ and a fold change of $\log|2FC| \geq 1$.

2.11. WGCNA

A scale-free network was constructed using the R-package WGCNA, employing soft thresholding to identify modules with distinct expression patterns. The soft threshold function was utilized to calculate power parameters. A dynamic cutting method was employed for the identification of co-expression gene modules, and gene dendrograms were generated through hierarchical clustering based on the dissimilarity of the topological overlap matrix. Finally, genes displaying similar expression profiles were clustered into the network graph.

2.12. Assessment of protein expression of IL-17 and p-IKKα in colon tissues via immunohistochemistry

Paraffin sections of colon tissues fixed with 4 % paraformaldehyde weresubjected to antigenic repair, followed by blocking with 10 % goat serum for 1 h. The primary antibody was applied and incubated overnight at 4 °C. Subsequently, the sections were incubated with a secondary antibody for 60 min, followed by dropwise staining with DAB solution and subsequent hematoxylin re-staining. The sections were dehydrated and sealed for microscopic examination (Liu et al., 2023).

2.13. WB analysis of IL-17A, p-P65 inflammatory factors in colon tissues

The colon tissue was incorporated into the prepared tissue lysate and kept on ice for mixing. Subsequently, it was centrifuged at 13,000 rpm

for 10 min at 4 °C, and the supernatant was collected. Sample proteins were separated through sodium dodecyl sulfate–polyacrylamide gel electrophoresis (SDS-PAGE) before being transferred onto a polyvinylidene fluoride (PVDF) membrane. This membrane was subsequently blocked with 5 % skimmed milk powder for 1 h, followed by overnight incubation with primary antibodies (IL-17A, P65, p-P65, β-actin) at 4 ℃. The following day, the membrane was washed with a Tris-buffered saline Tween (TBST) solution and incubated with the secondary antibody for 1 h. Afterward, the membrane was washed three times with a TBST solution, followed by the preparation of an electrochemiluminescence (ECL) luminescent solution. Finally, protein bands on the membrane were visualized using a chemical imaging system (Duan et al., 2024).

2.14. Statistical analysis

GraphPad Prism 8.0 software was employed for the analysis of experimental data. Results were expressed as mean ± standard deviation, and the differences between the two groups were assessed using a one-way ANOVA. A threshold of $p < 0.05$ indicated statistical significance.

3. Results

3.1. Compositional results of REO

The REO components were analyzed through GC–MS, yielding the ion mass spectra depicted in Fig. S1 (A). The obtained results were subsequently cross-referenced with NIST14. Employing RI calculations for each n-alkane, in combination with relevant literature, we identified a total of 19 distinct REO components. Their respective structures are illustrated in Fig. S1(B–T), and with detailed information provide in Table S1.

3.2. REO-ME results

3.2.1. Preparation of REO-ME

The ME was prepared by combining the oil phase, water phase, surfactant, and co-surfactant in certain ratios. The larger area of the ME region in the lower left corner of the pseudo-ternary phase diagram indicates greater stability. These results are shown in Fig. 1 (A-E), illustrating the influence of five factors (surfactant, co-surfactant, temperature, KM, auxiliary oils) on the formation of REO-ME. Experimental data showed that the most extensive ME area was achieved when employing Tween-80 as the surfactant, anhydrous ethanol as the co-surfactant. isopropyl myristate (IPM) with REO (1:1) as the oil phase (REO accounted for 1.75 % of the REO-ME system), a 2:1 ratio of KM, and a preparation temperature of 25 °C.

3.2.2. Characterization of REO-ME

REO-ME exhibited clarity, and transparency, with a particle size of 14.14 ± 0.49 nm, and a polydispersity index was 0.082 ± 0.02, as shown in Fig. 1(F). The Zeta potential value was −5.013 ± 0.684 mV, as shown in Fig. 1(G). As shown in Fig. 1(H), transmission electron microscopy revealed spherical emulsion droplets with a neat shape and uniform distribution, with the size of the particles in accordance with the requirements. Additionally, the selection of Tween-80 prevented the coalescence of oil droplets (Shi et al., 2022). The diffusion rate of water-soluble methylene blue in the ME surpassed that of Sudan III. confirming that the prepared ME was of the O/W type, as shown in Fig. 1(L).

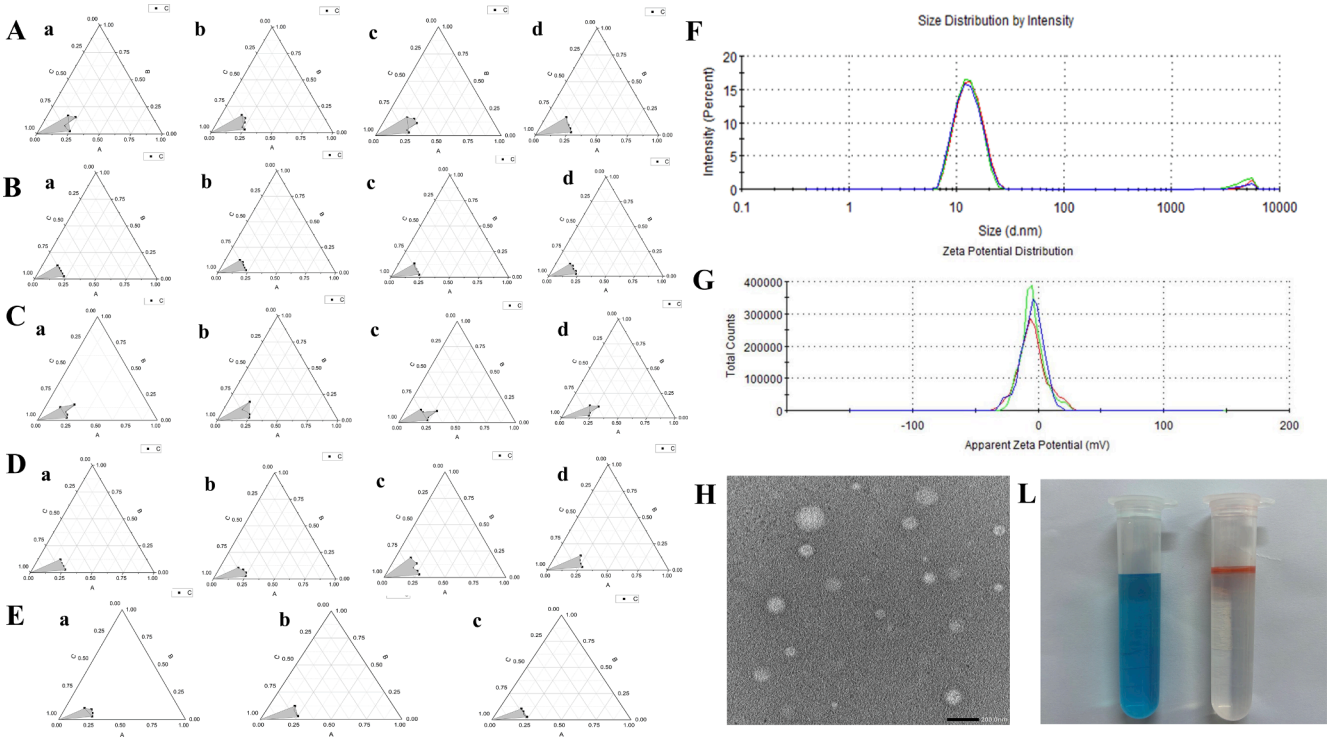

Fig. 1. REO-ME characterization. (A) Surfactants: a, castor oil polyoxyethylene ether (EL-40); b, polyoxyethylene hydrogenated castor oil (RH-40); c, Tween-80; d, Tween-20. (B) Co-surfactants: a, 1,2 propylene glycol; b, polyethylene glycol-400 (PEG-400); c, anhydrous ethanol; d, glycerine. (C) Temperatures: a, 25 °C; b, 30 °C; c, 40 °C; d, 50 °C. (D) KM: a, 1:1; b, 2:1; c, 3:1; d, 4:1. (E) Oil phase: a, IPM; b, isopropyl hexadecanoate (IPP); c, oleic acid. The ME areas formed by the four surfactants were $S_{RH\text{-}40} = 0.00069$, $S_{EL\text{-}40} = 0.00015$, $S_{Tween\text{-}80} = 0.00439$, and $S_{Tween\text{-}20} = 0.00044$. The area of the regions formed by the four co-emulsifiers was $S_{1,2\text{-}propanedio} = 0.000019$, $S_{PEG\text{-}400} = 0.000337$, $S_{anhydrous\ ethanol} = 0.000676$, and $S_{glycerine} = 0.000613$. The area of MEs formed by the four preparation temperatures was $S_{25°C} = 0.0042$, $S_{30°C} = 0.0033$, $S_{40°C} = 0.00408$, and $S_{50°C} = 0.0030$. The KM values of the four types were $S_{1:1} = 0.00025$, $S_{2:1} = 0.00133$, and $S_{3:1} = 0.00089$, $S_{4:1} = 0.00093$. The ME area formed by the three auxiliary oil was $S_{IPP} = 0.00083$, $S_{IPM} = 0.0018$, and $S_{oleic\ acid} = 0.00075$. (F) REO-ME particle size. (G) REO-ME Zeta potential map. (H) REO-ME transmission electron microscopy map. (L) REO-ME type identification map.

3.3. Effect of various REO concentrations on RAW264.7 cell viability

The efficacy and cell viability of the drug can be evaluated by cytotoxicity. As a study of food function, the most important thing is to investigate the safety of the research object (Liu et al., 2021b). In this study, the toxicity of REO and REO-ME on RAW264.7 cells was evaluated by MTT experiment, as shown in Fig. 2(A), cell viability exceeded 95 % at REO concentrations of 0.5–1.0 μg/mL. Therefore, these concentrations were employed for subsequent experiments. The survival rate of REO-ME against RAW264.7 cells at 0.5–2.0 μg/mL was greater than 95 %, as shown in Fig. S2(A). The control ME was used as a carrier, indicating that cytotoxicity would not be induced, as shown in Fig. S2 (B). In this study, REO-ME was less cytotoxic than REO at the same concentration.

3.4. Effect of various concentrations of REO on NO content in RAW264.7 cells

Measurement of NO content indicated that, compared to the control group, the model group exhibited a significantly higher NO content. Conversely, the administered group displayed a significantly lower NO content compared to the model group, as shown in Fig. 2(B). These results indicate that REO could effectively reduce the expression of the inflammatory factor NO.

3.5. Pharmacodynamic evaluation of REO and REO-ME

3.5.1. DAI score in mice

On the third day of the modeling process, mice began exhibiting associated with UC. Feces became dilute, adhering to the anus, with the appearance of blood in stools on the fourth day. Additionally, mice displayed rough fur, weight loss, and decreased water intake. In the REO and REO-ME groups, mice gradually began to regain weight from the fifth day onward. The consistency of feces-stools gradually became normal, occasionally showing traces of blood. The DAI scores for each group are shown in Fig. 2(C), indicating the efficacy of both REO and REO-ME in alleviating UC in mice, with REO-ME group exhibiting superior therapeutic effect compared to the REO group.

3.5.2. Serum IL-6 and TNF-α concentrations

To investigate the therapeutic effects of REO and REO-ME on UC, we assessed the concentration of IL-6 and TNF-α in the serum of mice. Compared to the control group, the model group exhibited a significant increase in both IL-6 and TNF-α concentrations. Conversely, the REO and REO-ME groups demonstrated a significant decrease in IL-6 and TNF-α concentration compared to the model group, as illustrated in Fig. 2(D, E). These experimental results showed that both REO and REO-ME could reduce the expression of the inflammatory factors, with a more significant effect observed in the REO-ME group.

3.5.3. HE staining results

The HE staining results for each group of mice are presented in Fig. 1 (F). In the control group, the colonic tissue exhibited a generally normal structure, with well-organized cells in the mucosal layer and an abundance of cup-shaped cells interspersed among the epithelial cells. Conversely, the model group displayed disrupted colon tissue structure, characterized by inflammatory cell infiltration in the mucosal layer, along with mucosal congestion and edema. In contrast, the drug-administered group exhibited a more orderly arrangement of colon mucosal layer cells, along with the presence of cup-shaped cells between epithelial cells. These observations indicated that both REO and REO-ME could treat UC in mice.

3.6. Network pharmacology results

3.6.1. Identification of key targets

A total of 397 REO targets were obtained from the Swiss Target-Prediction database, while 5,548 targets associated with UC were obtained from the DisGeNET, Genecards, and OMIM databases. Additionally, we identified 1,524 differentially expressed genes from the

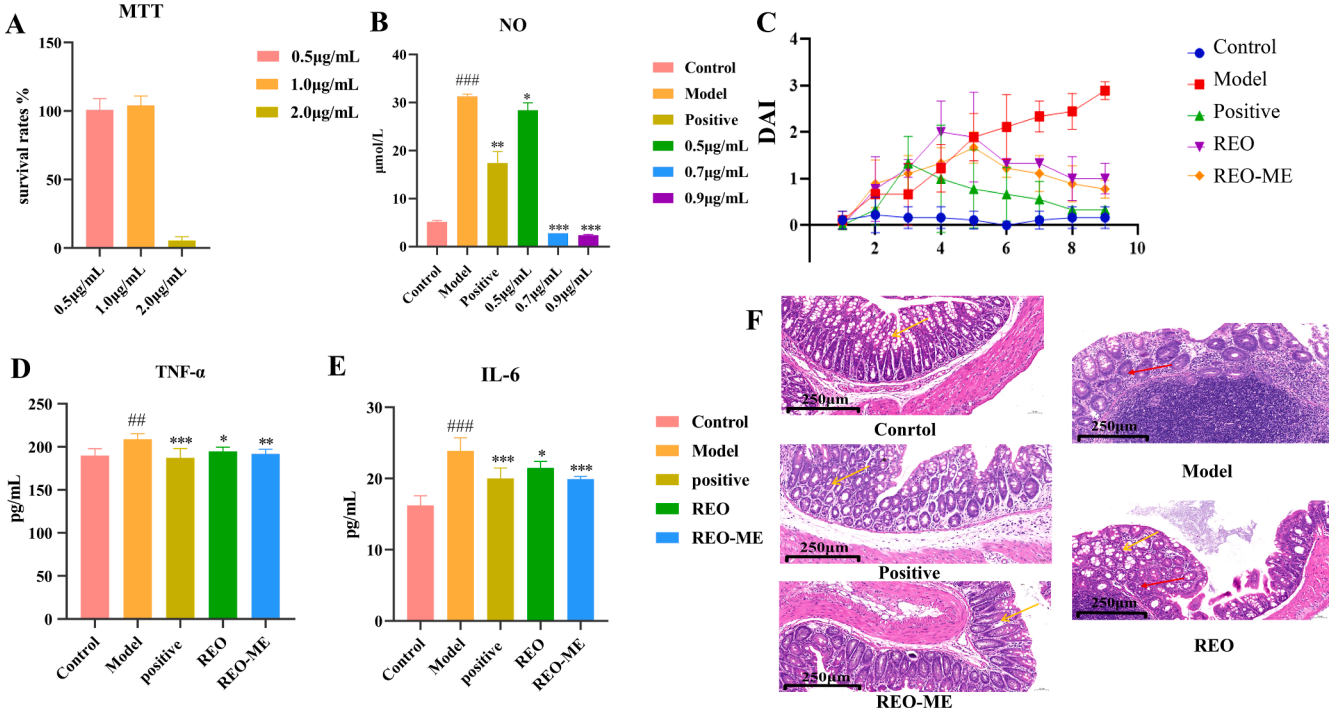

Fig. 2. (A) MTT assay results. (B) NO concentrations. ###$p < 0.001$vs control, *$p < 0.05$, **$p < 0.01$, ***$p < 0.001$vs model. (C) DAI scores in mice. (D, E) TNF-α, IL-6 ELISA results (n = 6). ##$p < 0.01$, ###$p < 0.001$ vs control group, *$P < 0.05$, **$P < 0.01$, ***$p < 0.001$ vs model group. (F) HE staining of mouse colons (yellow arrowheads indicate cup-shaped cells, and red arrows indicate inflammatory cell infiltration). (For interpretation of the references to colour in this figure legend, the reader is referred to the web version of this article.)

GEO dataset, with upregulated genes highlighted in red and downregulated genes in highlighted green in Fig. 3(E). Subsequently, a total of 40 genes were found to overlap among the REO components, disease-related targets, and GEO data, as shown in Fig. 3(B). These 40 key targets were imported into Cytoscape 3.7.2 for visualization, as presented in Fig. 3(F), and the targets with the highest degree values included IL-6, TNF, PTPRC, STAT3, chemokine ligand 8 (CXCL8), and PTGS2, among others.

3.6.2. Biological pathway enrichment analysis

The R software was utilized to conduct enrichment analyses on the set of 40 target proteins. Subsequently, alterations in the outcomes of both GO and KEGG analyses were observed upon the incorporation of weights. Specifically, the analysis yielded 790 entries for biological processes (BP), 6 entries or cellular components (CC), 44 entries for molecular functions (MF), and a total of 76 KEGG pathways. Among the top three BP entries, the initial classifications of "neuroinflammatory response", "regulation of inflammatory response", and "microglia activation" were replaced with "lipolysis", "steroid metabolism", and "fatty acid metabolism", respectively. In terms of KEGG pathways, the initial top three pathways, "hepatitis B", "coronavirus-COVID-19", and "IL-17 signaling pathway", were replaced with "IL-17 signaling pathway", "nitrogen metabolism", and "PPAR signaling pathway", respectively. The IL-17 signaling pathway ascended from the third position to the first, underscoring its significance (Fig. 3[H]).

3.7. Molecular docking

The components of three targets in the IL-17 signaling pathway, namely HSP90AA1, IKBKB, RELA, and REO, were selected for molecular docking studies using the characterized ligands geldanamycin, tamoxifen, and fostamatinib in the LibDock module of Discovery Studio. The results showed relatively high binding affinity between HSP90AA1 and L-α-terpineol, IKBKB and α-pinene, and RELA and eucalyptol. These results indicate that L- alpha -terpineol, alpha -pinene, and eucalyptol are key components of REO, showing potential for the treatment of UC.

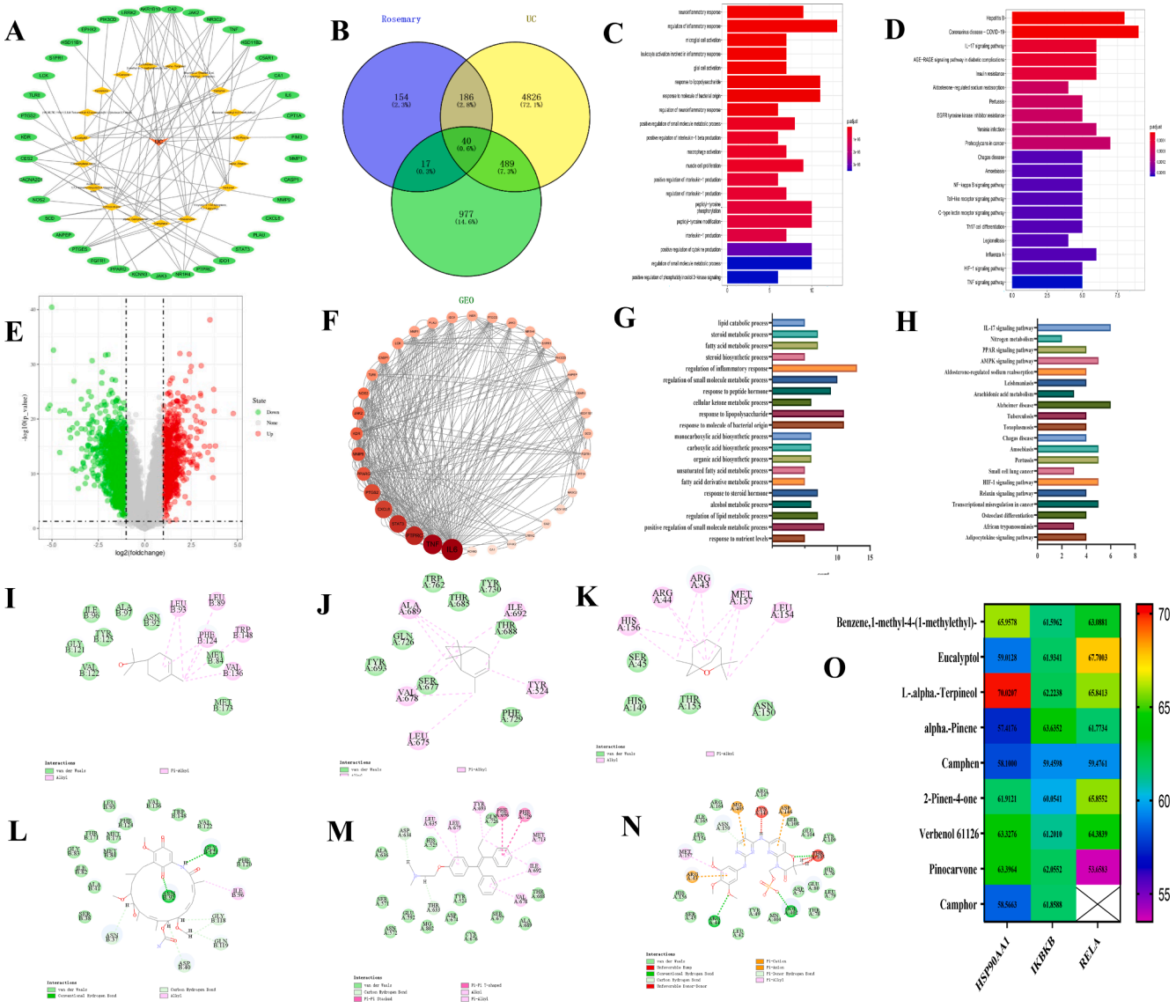

Fig. 3. Network pharmacology diagrams. (A) REO component-UC-key target network diagram. (B) REO target-UC target-GEO differential gene Venn diagram. (C, D) GO-BP and KEGG pathway enrichment analysis results prior to sorting. (E) A volcano plot of differential genes. (F) Visualization of key target PPI. (G, H). Results of GO-BP and KEGG pathway enrichment analysis after classification. (I–K) The docking results for HSP90AA1, IKBKB, and RELA, with the components L-alpha-terpineol, alpha -pinene, and eucalyptol, respectively. (L–N) The docking results for HSP90AA1, IKBKB, and RELA with the characterized ligands. (O) Heat map of molecular docking results.

The corresponding results are shown in Fig. 3(I-O), and detailed docking scores can be found in Table S2.

3.8. REO-ME pharmacodynamic analysis results

3.8.1. Changes in DAI score and colon length in mice

The control group of mice remained in a normal state, exhibiting no discernible changes in their diet, water consumption, or body weight. In contrast, starting from the second day, mice in the model group began to display weight loss, loose feces, diarrhea, and blood in their stool on the fourth day. These symptoms persisted until the end of the experiment. However, mice in the administered group receiving treatment exhibited varying degrees of symptom reduction and a significant decrease in DAI scores, as shown in Fig. 4(A). The colon length of mice in each group is presented in Fig. 4(B). Compared to those in the control group, mice in the model group had shorter colons, while mice in the administered group demonstrated longer colons than those in the model group. These results suggest that REO-ME has the potential to alleviate DSS-induced UC.

3.8.2. Serum concentrations of TNF-α, IL-6, IL-17, and IL-1β in mice

The results of ELISA are shown in Fig. 4(C). Concentrations of TNF-α, IL-6, IL-17, and IL-1β were significantly higher in the model group compared to those in the control group. Moreover, the serum concentrations of TNF-α, IL-6, IL-17, and IL-1β were significantly decreased in the REO-ME groups compared to those in the model group. These results suggest that REO-ME reduces inflammatory factor expression in the serum.

3.9. Transcriptome sequencing analysis

Leveraging pharmacodynamic data, we analyzed the mechanism of action in treating REO-ME in treating UC across the control, model, and REO-ME high-dose groups. Using a threshold of $P < 0.05$ and $|\log_2 FC| > 1$ as the criteria for judgment, we identified a total of 3,268 genes that exhibited significant differential expression. Among these, 1,581 genes were upregulated and 1,687 were downregulated. The sample clustering is illustrated in Fig. 5(A), and the differential gene expression between the control and model groups is illustrated in a volcano plot in Fig. 5(B). GO analysis of differential genes revealed enrichment in 22 BP, 7 MF, and 14 CC, as shown in Fig. 5(C). KEGG analysis of REO-ME regulation showed that the genes were enriched in a total of 337 pathways, primarily in the TNF and IL-17 signaling pathways, as shown in Fig. 5(E).

3.10. WGCNA results

A scale-free network was constructed with a soft threshold of eight. Fig. 6(A) displays the R^2 fit index for the scale-free network across various thresholds, with the blue and red horizontal lines representing correlation coefficients of 0.8 and 0.9, respectively. In total, 19 gene modules were identified in this network, as illustrated in Fig. 6(B). Analysis revealed that the tan module contained the most genes, totaling 6,858, as shown in Fig. 6(C). In the correlation heatmap between the modules (Fig. 6[D]), the darker colors of the squares, indicate stronger correlations. Fig. 6(E) illustrates the relationship between traits and modules, with red indicating positive correlations and green indicating negative correlations. Additionally, Fig. 6(F) presents the correlation heatmap between the modules and individual genes, with darke colors at each point signifying stronger correlations. Subsequently, KEGG enrichment analysis was performed on the tan module, which exhibited the highest number of genes. The results are shown in Fig. 6(H), where in the IL-17 signaling pathway ranked high, securing the sixth position. This indicates that the IL-17 signaling pathway may be a key pathway involved in the therapeutic effect of REO-ME in UC.

3.11. Immunohistochemical results

The immunohistochemical results are presented in Fig. 7(A–C). Compared to the control group, the model group exhibited significantly elevated levels of the inflammatory factors p-IKKα and IL-17. Conversely, compared to the model group, the high-dose REO-ME group demonstrated a significant reduction in the expression of p-IKKα and IL-17. These results suggest that REO-ME may effectively treat of UC by modulating the expression of IKKα and IL-17 in colonic tissues.

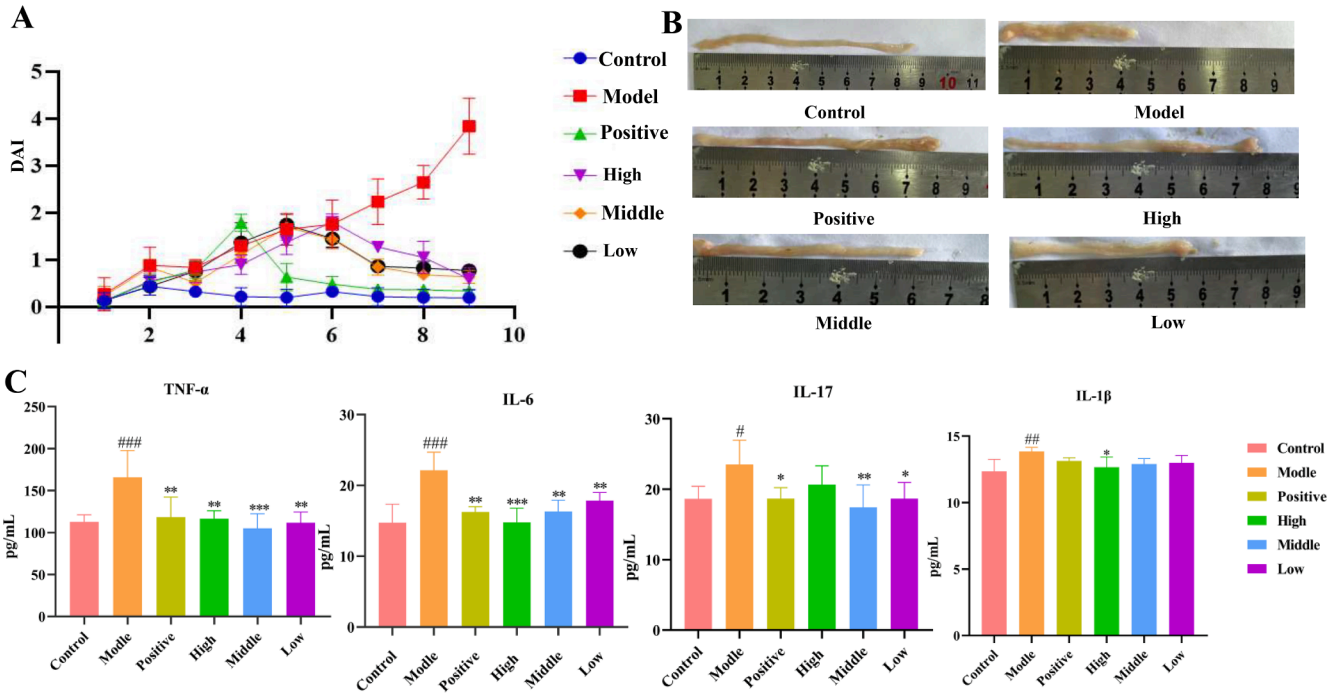

Fig. 4. Pharmacodynamic results of REO-ME. (A) DAI scores of REO-ME for UC. (B) Mouse ELISA results from left to right for TNF-α, IL-6, IL-17, and IL-1β. (C) Immunohistochemistry results. $^{\#}P < 0.05$, $^{\#\#}P < 0.01$, $^{\#\#\#}P < 0.001$vs control group, $^{*}P < 0.05$, $^{**}P < 0.01$, $^{***}P < 0.001$vs model group.

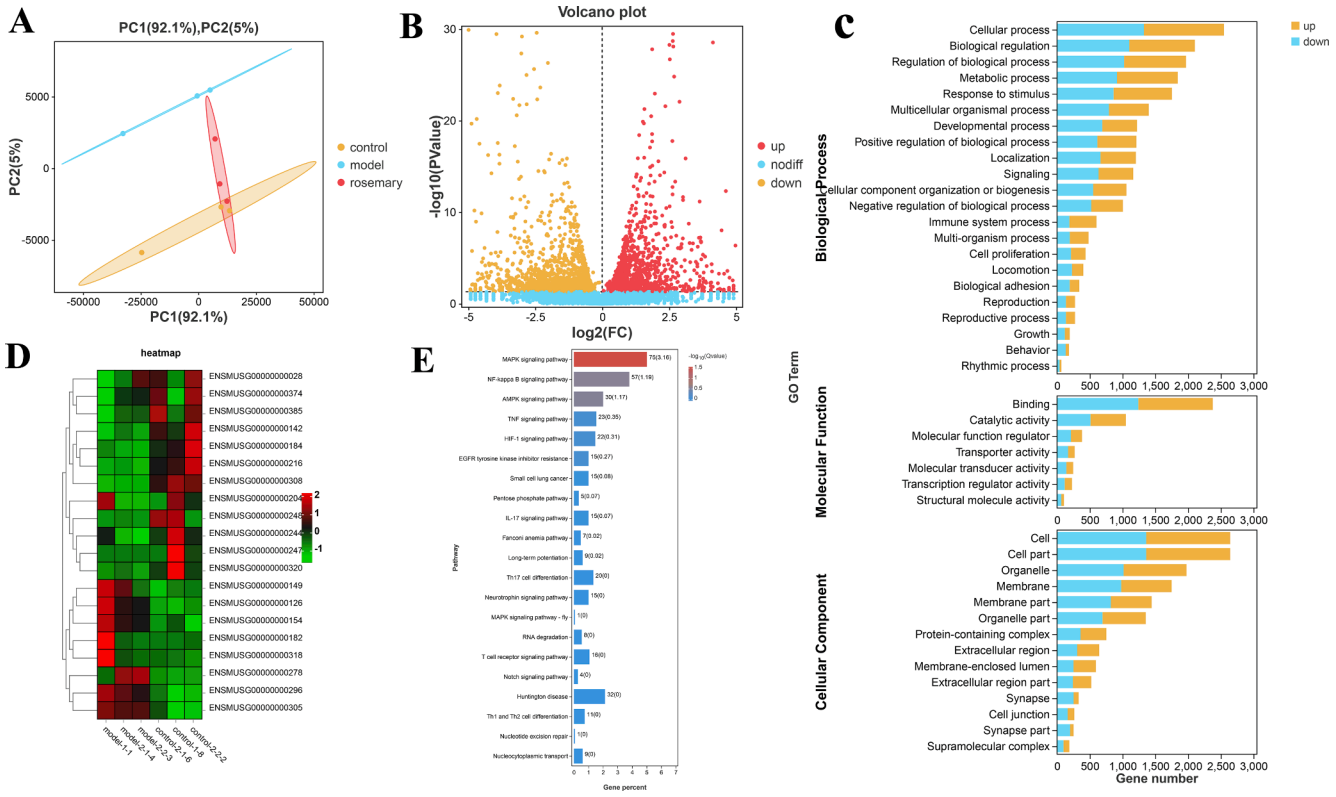

Fig. 5. Transcriptome analysis. (A) PCA clustering analysis plot. (B) A volcano plot of differential genes. (C) GO enrichment analysis of differential genes. (D) A heatmap of differential genes. (E) Differential gene KEGG enrichment results.

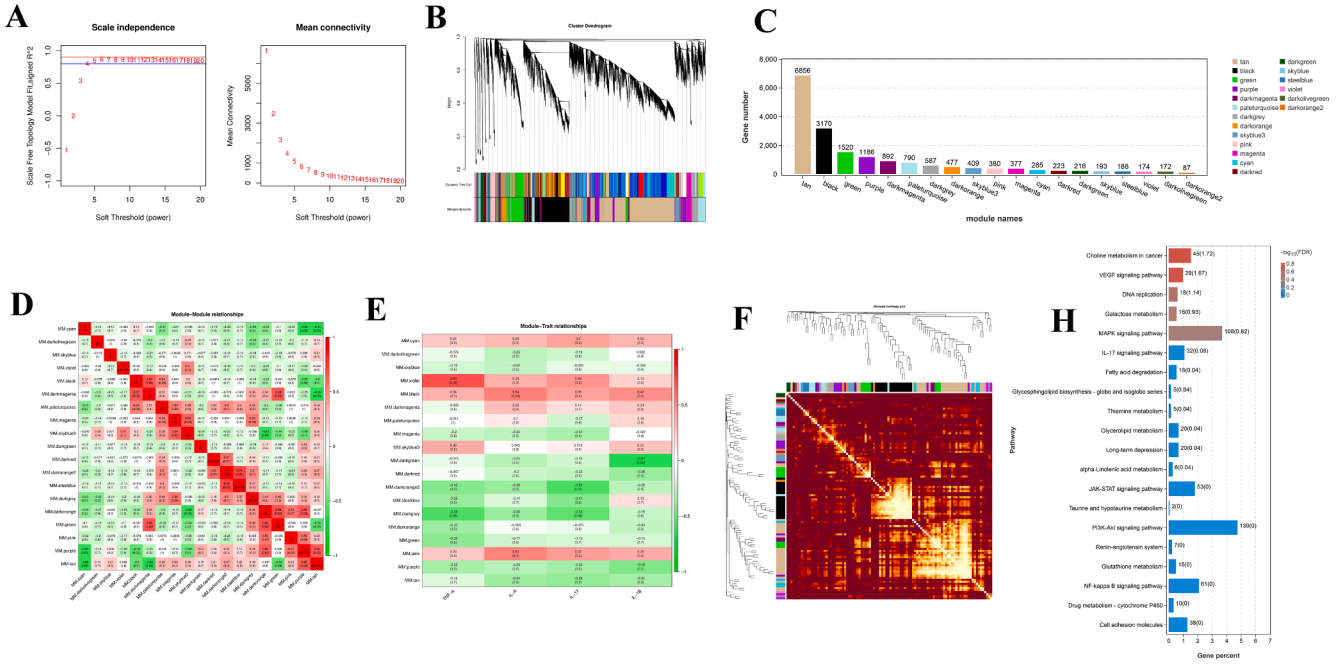

Fig. 6. Results of the WGCNA. (A) Relationship between soft threshold and network graph. (B) Gene clustering dendrogram. (C) Module overview graph. (D) Inter-module correlation analysis. (E) Results of correlation analysis of trait modules. (F) Correlation between genes and modules. (H) KEGG analysis of the tan module.

3.12. REO-ME modulates the expression of key proteins on the IL-17 pathway

As shown in Fig. 7(D), WB analysis demonstrated a significant increase in the protein expression levels of IL-17 and p-P65 in the model group compared to the control group. Compared with the model group, the protein expressions of IL-17 and p-P65 in the colon of mice in the REO-ME groups was significantly decreased.

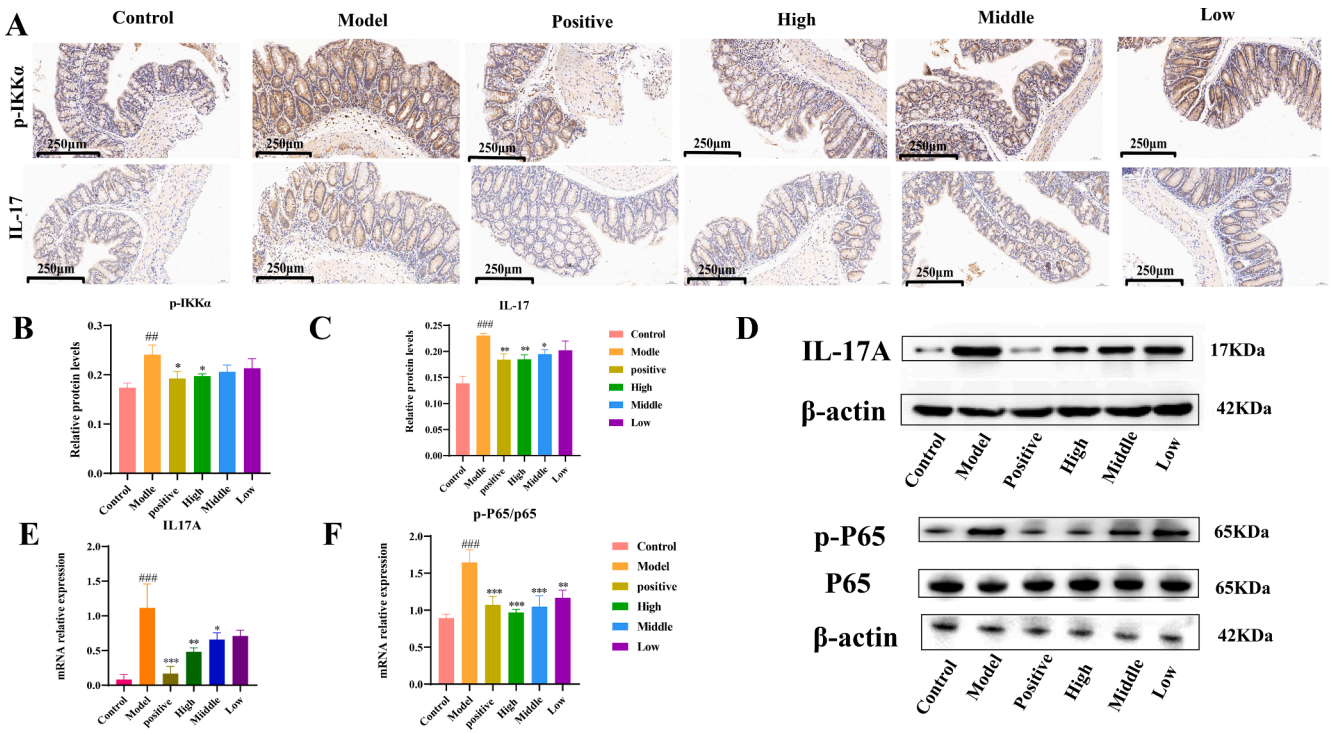

Fig. 7. (A) Immunohistochemical results. (B, C) Statistical analysis of p-Ikkα and IL-17A, (D) WB results of IL-17A/β-actin, p-P65/P65 levels. (E, F) The expression levels of IL-17A, p-P65, P65, and β-actin. $^{\#\#}P<0.01$, $^{\#\#\#}P < 0.001$vs control group, $^{*}P < 0.05$, $^{**}P < 0.01$, $^{***}P < 0.001$vs model group.

4. Discussion

The treatment of RAW264.7 cells with LPS is widely employed in inflammation studies (Xiang et al., 2015). In this study, utilizing the MTT assay, we observed that cell viability exceeded 95 % at REO concentrations of 0.5–1.0 μg/mL. Subsequently, we induced cellular inflammation using LPS and found that REO effectively inhibited the expression of the inflammatory cytokine NO. The area of the ME region by depicted in the pseudo-ternary phase diagram indicates stability and the capacity to load essential oils. These results, revealed that the optimal formulation of REO-ME involves a combination of Tween-80, anhydrous ethanol, IPM: REO (1:1), and water at 25 °C in a certain ratio. Tween-80, a widely employed surfactant in food and industrial applications, exhibits minimal irritation and hemolysis. According to the literature, anhydrous ethanol is primarily used as a co-surfactant in the preparation of microemulsions (Chen et al., 2013; Liang et al., 2020) and are inexpensive, hydrophilic, safe and non-toxic, and are currently used in multiple fields (Li et al., 2019). IPM has low irritation and low toxicity (Shi et al., 2022) and is used in the preparation of microemulsions (Karadağ et al., 2022). Zeta potential measures the stability of microemulsions and characterizes the surface charge of the emulsion. It has been found that the zeta value changes under different conditions, which affects the stability of microemulsions. In this paper, the zeta value was −5.013 ± 0.684 mV, which is consistent with the characterization results of curcumin nanoemulsions (Sari et al., 2015). REO is unstable and volatile. As shown in Fig. S3 (A-B), the release rate of REO was 1.91 % when REO-ME was placed at 25 ℃ for 24 h. Based on the experimental results, it was hypothesized that the sealed storage of REO-ME at 4 ℃ might improve its stability (Yan et al., 2023).

The DSS-induced UC model is a common animal model. In this study, we found improvements in fecal blood and an increase in body in mice treated with REO-ME and REO. The experimental results showed a more significant reduction in the serum concentration of the inflammatory factors IL-6 and TNF-α in REO-ME-treated mice compared to REO. This may be attributed to the excellent drug dispersion, bioavailability, and stability of the ME, potentially mitigating issues associated with the volatility and limited oral absorption of essential oils (Kim et al., 2017; Zeng et al., 2010). To delve deeper into the mechanistic action of REO-ME in the DSS-induced UC model in mice, we assessed mouse colon length, performed immunohistochemical analysis of IKKα and IL-17 expression in the colon, and ascertained the levels of the inflammatory factors TNF-α, IL-6, IL-17, and IL-1β in the serum, with assessment of the protein expression of IL-17A in colon tissue as validation criteria. The experimental results showed a significant reduction in the expression of inflammation-related proteins and the concentration of serum inflammatory factors in the colon of mice following administration of REO-ME. Therefore, we posit that the treatment of UC with REO-ME is associated with the regulation of the expression of p-IKKα, IL-6, IL-17, IL-1β, and p-P65.

Network pharmacology, in conjunction with GEO, revealed 40 key targets, which were subsequently ranked based on their degree values. The top-ranking targets encompassed IL-6, TNF, PTPRC, STAT3, CXCL8, and PTGS2, among others. IL-6 and TNF are recognized as pro-inflammatory factors associated with UC (Zhang & Shi, 2020). Although IL-6 can aid the host resisting acute environmental stress, prolonged IL-6 expression leads to a range of inflammatory responses (Pinci et al., 2020; Rose-John, 2012; Tanaka & Kishimoto, 2012). TNF, a central mediator of inflammation, exerts a pro-inflammatory influence, and inhibiting TNF effectively prevents the development of colitis (Bejeshk et al., 2022; Pinci et al., 2020). In addition, CXCL8, released in response to IL-1 has been implicated in the development of inflammation (Wei et al., 2018). These findings suggest a close association between these targets and the therapeutic potential of REO-ME in UC. Subsequently, we reevaluated the KEGG enrichment results by incorporating OB values. This reordering placed the IL-17 signaling pathway the forefront, previously ranked third. In addition, utilizing transcriptome sequencing to analyze differential genes, and KEGG pathway analysis of the most gene-enriched tan module revealed that most of the enriched pathways were associated with inflammation, with the IL-17 signaling pathway being a prominent component among these pathways. Based on the integrated approach of network pharmacology and transcriptome analysis, we postulate that the IL-17 signaling pathway

may play a pivotal role in the mechanism of REO-ME in the treatment of UC.

To further explore the role of the active ingredient in REO-ME in the IL-17 signaling pathway, we conducted additional validation through molecular docking. The docking scores revealed superior binding affinities of HSP90AA1, IKBKB, RELA, and the active ingredients, along with their characterized ligands. The results provided further evidence that L-alpha-terpineol, alpha-pinene, and eucalyptol were the key active components of REO-ME for managing UC. L-alpha-terpineol is a natural epoxide monoterpene with recognized anti-inflammatory and antioxidant properties. It exerts its inhibitory effects on UC by modulating NF-κB, TNF-α, among others, thereby inhibiting the release of pro-inflammatory cytokines. RELA is a member of the NF-κB family, and NF-κB/RELA overactivation has been implicated in IBD (Yin et al., 2023). Therefore, we postulate that the active ingredients in REO-ME mitigate UC by modulating key targets of the IL-17 signaling pathway.

IL-17 represents a class of inflammatory factors produced by the Th17. Receptor IL-17R, which consists of five related proteins, namely IL-17R (A–E). Among them, IL-17RA and IL-17RC bind to IL-17A and IL-17F, orchestrating cellular responses (Levin, 2009). Upon binding to their respective receptors, IL-17 activates the NF-κB cascade, leading to the release of the pro-inflammatory factors IL-6, TNF-α, and IL-1β, thereby promoting inflammation (Geremia & Jewell, 2012; Zhou et al., 2021). NF-κB activating factor 1 (Act1) serves as a crucial intermediary connecting the IL-17 signaling pathway with TNF-related factor 6 (TRAF6). Additionally, HSP90 interacts with Act1 to facilitate downstream IL-17 signaling. A decrease in Act1 activity inhibits the NF-κB pathway downstream of the IL-17 signaling cascade, resulting in diminished inflammation (Swaidani et al., 2019; Wu et al., 2014). Studies have shown that TRAF6 binds to the TAK1 complex, subsequently activating the IKK complex, which in turn leads to NF-κB activation and the regulation of the inflammatory factors TNF-α and IL-6. Therefore, this study proposes that REO-ME treats UC by targeting HSP90AA1 through its constituent L-alpha-terpineol. This action disrupts the interaction between Act1 and TRAF6, consequently inhibiting the activation of the IKK complex. Simultaneously, alpha-pinene acts on IKKB, inhibiting its phosphorylation. When IKKB is downregulated, in conjunction with the effect of eucalyptole on the target RELA, the activation of NF-κB is suppressed. This regulation influences the expression of downstream the inflammatory factors such as TNF-α, and IL-6, et, thereby inhibiting the IL-17 signaling pathway and yielding a therapeutic effect on UC (Liu et al., 2021a). This mechanism is illustrated in Fig. 8.

In summary, this study introduced weighting coefficients for both the OB and ingredient content, utilizing traditional network pharmacology principles to model the compositional changes of drugs in vivo. This approach enhances the objectivity and accuracy of experimental outcomes. Therefore, we hypothesize that the mechanism underlying the therapeutic action of REO-ME in treating UC may involve the effects of L-alpha-terpineol, alpha-pinene, and eucalyptole on the targets HSP90AA1, IKBKB, and RELA, thereby inhibiting the expression of pro-inflammatory factors such as TNF-α, IL-17, IL-6, and IL-1β in the IL-17 signaling pathway. This Indicates that REO-ME therapy for UC operates through a multi-component, multi-target, and multi-pathway. Nonetheless, our study exhibits many shortcomings. The consistent anti-inflammatory effect observed across REO components, as evidenced the results of network pharmacology and molecular docking warrants further investigation. Subsequent monomeric anti-inflammatory pharmacodynamic studies should be conducted to validate the specific anti-inflammatory effects of each REO component. In addition, we only initially discussed the preparation method of REO-ME and did not study the variation of the content of each component in REO-ME. The content of anhydrous ethanol, a volatile component in REO-ME, should be determined in future studies.

5. Conclusion

In this study, we investigated the therapeutic potential of REO-ME on

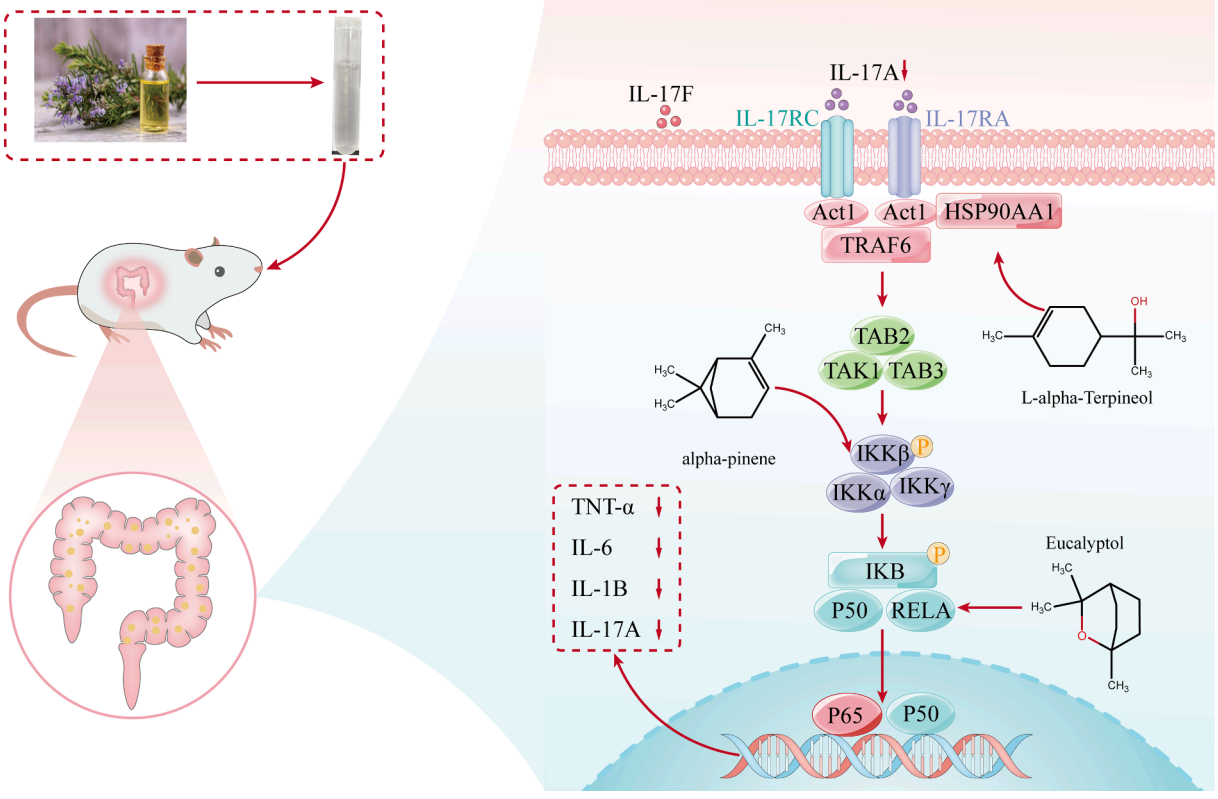

Fig. 8. Diagram of the mechanism of action of REO-ME.

DSS-induced US through combining network pharmacology, transcriptomics technology and WGCNA. Through pharmacodynamic experiments, we further elucidated the mechanism of action of REO-ME on US. The results showed that L-alpha- terpineol, alpha-pinene and eucalyptol in REO-ME inhibited the release of inflammatory factors by modulating the key targets within the IL-17 signaling pathway, HSP90AA1, IKBKB, and RELA, treating UC. Given the wide range of applications of rosemary in our daily life, the preparation of rosemary into oral microemulsions can be used to develop and utilize anti-inflammatory effects of functional foods or nutritional supplements, providing a new direction for the treatment of ulcerative colitis with rosemary.

Ethics statement

In this paper, all animal experiments were approved by the Ethics Committee of Shaanxi University of Chinese Medicine. (Ethics No.: SUCMDC20210520001).

CRediT authorship contribution statement

Jie Wang: Conceptualization, Writing – original draft. **Yanzhuo Jia:** Conceptualization, Writing – original draft. **Ning Xia:** Conceptualization, Writing – original draft. **Xuan Wang:** Data collation. **Peijie Zhou:** Data collation. **Jiawei Duan:** Data collation. **Jinkai Li:** Data collation. **Taotao Li:** Methodology, Software. **Tiantian Tang:** Methodology, Software. **Yujiao Wang:** Methodology, Software. **Ding Liu:** Methodology, Software. **Huanxian Shi:** Validation, Formal analysis, Survey. **Yundong Xie:** Validation, Formal analysis, Survey. **Chongbo Zhao:** Validation, Formal analysis, Survey. **Jing Sun:** Funding acquisition, Writing – original draft. **Xiaofei Zhang:** Funding acquisition, Writing – original draft.

Declaration of competing interest

The authors declare that they have no known competing financial interests or personal relationships that could have appeared to influence the work reported in this paper.

Data availability

Data will be made available on request.

Acknowledgements

The authors gratefully acknowledge the financial supports by the National Natural Science Foundation of China (81703720), the National Key Research and Development Program (2021YFD1601004), Project of Shaanxi Provincial Department of science and technology (2022JM-555), Key R & D program of Xianyang City (2021ZDYF-SF-0015), Shaanxi Provincial Bureau of Chinese Medicine (ZYJXG-Y23005), Shaanxi Provincial Administration of Traditional Chinese Medicine "Qin Medicine" Development Key Research Project (2021-02-22-014), Xi'an Science and Technology Bureau Project (23CXLHTJSGG0004-2023), Shaanxi Provincial University Engineering Research Center of Chinese Medicine Aromatic Industry, Youth Innovation Team of Aromatic Chinese Medicine Industrialization Key Technology, and Shaanxi Provincial Engineering and Technology Research Centre for Chinese herbal medicine.

Appendix A. Supplementary data

Supplementary data to this article can be found online at https://doi.org/10.1016/j.jff.2024.106180.

References

Akhbari, M., Masoum, S., Aghababaei, F., & Hamedi, S. (2018). Optimization of microwave assisted extraction of essential oils from Iranian Rosmarinus officinalis L. using RSM. *Journal of Food Science and Technology, 55*(6), 2197–2207. https://doi.org/10.1007/s13197-018-3137-7

Bejeshk, M. A., Aminizadeh, A. H., Rajizadeh, M. A., Khaksari, M., Lashkarizadeh, M., Shahrokhi, N., Zahedi, M. J., & Azimi, M. (2022). The effect of combining basil seeds and gum Arabic on the healing process of experimental acetic acid-induced ulcerative colitis in rats. *Journal of Traditional and Complementary Medicine, 12*(6), 599–607. https://doi.org/10.1016/j.jtcme.2022.08.001

Brindisi, M., Bouzidi, C., Frattaruolo, L., Loizzo, M. R., Tundis, R., Dugay, A., Deguin, B., Cappello, A. R., & Cappello, M. S. (2020). Chemical profile, antioxidant, anti-inflammatory, and anti-cancer effects of italian salvia rosmarinus spenn. *Methanol Leaves Extracts. Antioxidants (Basel), 9*(9). https://doi.org/10.3390/antiox9090826

Caprilli, R., Viscido, A., & Latella, G. (2007). Current management of severe ulcerative colitis. *Nature Clinical Practice. Gastroenterology & Hepatology, 4*(2), 92–101. https://doi.org/10.1038/ncpgasthep0687

Chen, L., Zhao, X., Cai, J., Guan, Y., Wang, S., Liu, H., Zhu, W., & Li, J. (2013). Triptolide-loaded microemulsion-based hydrogels: Physical properties and percutaneous permeability. *Acta Pharmaceutica Sinica B, 3*(3), 185–192. https://doi.org/10.1016/j.apsb.2013.05.001

Ding, Z., Zhou, L., & Fang, S. (2009). Application of Polyglycerol Diisostearate Ethoxylates in Microemulsion. *Journal of Dispersion Science and Technology, 30*(9), 1342–1349. https://doi.org/10.1080/01932690902735579

Duan, J., Li, J., Wang, Y., Zhou, P., Wang, X., Xia, N., Wang, J., Li, J., Wang, W., Wang, X., Sun, J., Guo, D., Zou, J., Zhang, X., & Wang, C. (2024). Therapeutic effects and mechanism of action of lavender essential oil on atopic dermatitis by modulating the STAT3/RORγt pathway. *Arabian Journal of Chemistry, 17*(2), Article 105525. https://doi.org/10.1016/j.arabjc.2023.105525

Fareed, S. A., Yousef, E. M., & Abd El-Moneam, S. M. (2023). Assessment of effects of rosemary essential oil on the kidney pathology of diabetic adult male albino rats. *Cureus, 15*(3), e35736. https://doi.org/10.7759/cureus.35736

Fletcher, J. M., Moran, B., Petrasca, A., & Smith, C. M. (2020). IL-17 in inflammatory skin diseases psoriasis and hidradenitis suppurativa. *Clinical and Experimental Immunology, 201*(2), 121–134. https://doi.org/10.1111/cei.13449

Gao, S., Li, Y., Wu, D., Jiao, N., Yang, L., Zhao, R., Xu, Z., Chen, W., Lin, X., Cheng, S., Zhu, L., Lan, P., & Zhu, R. (2022). IBD subtype-regulators IFNG and GBP5 identified by causal inference drive more intense innate immunity and inflammatory responses in CD than those in UC. *Frontiers in Pharmacology, 13*, Article 869200. https://doi.org/10.3389/fphar.2022.869200

Geremia, A., & Jewell, D. P. (2012). The IL-23/IL-17 pathway in inflammatory bowel disease. *Expert Review of Gastroenterology & Hepatology, 6*(2), 223–237. https://doi.org/10.1586/egh.11.107

Grace, M. H., Hoskin, R., Xiong, J., & Lila, M. A. (2021). Whey and soy proteins as wall materials for spray drying rosemary: Effects on polyphenol composition, antioxidant activity, bioaccessibility after in vitro gastrointestinal digestion and stability during storage. *LWT, 149*, Article 111901. https://doi.org/10.1016/j.lwt.2021.111901

Hao, F., Peng, Y., & Zhao, L. (2021). Study on the mechanism of action of astragalus-goji berry medicine in the treatment of ulcerative colitis based on network pharmacology technique. *Journal of Shanghai University of Engineering and Technology, 35*(04), 377–382.

Jampilek, J., & Kralova, K. (2022). Anticancer applications of essential oils formulated into lipid-based delivery nanosystems. *Pharmaceutics, 14*(12). https://doi.org/10.3390/pharmaceutics14122681

Kim, K. T., Lee, J. Y., Park, J. H., Cho, H. J., Yoon, I. S., & Kim, D. D. (2017). Capmul MCM/Solutol HS15-based microemulsion for enhanced oral bioavailability of rebamipide. *Journal of Nanoscience and Nanotechnology, 17*(4), 2340–2344. https://doi.org/10.1166/jnn.2017.13314

Karadağ, A. E., Üstündağ Okur, N., Demirci, B., & Demirci, F. (2020). Rosmarinus officinalis L. essential oil encapsulated in new microemulsion formulations for enhanced antimicrobial activity. *J Surfact Deterg., 25*, 95–103. https://doi.org/10.1002/jsde.12549

Levin, S. D. (2009). IL-17 receptor signaling: Ubiquitin gets in on the act. *Science Signaling, 2*(92), pe64. https://doi.org/10.1126/scisignal.292pe64

Li, J., Duan, J., Wang, Y., Zhou, P., Wang, X., Xia, N., Wang, J., Li, J., Wang, W., Wang, X., Sun, J., Guo, D., Zou, J., Zhang, X., & Wang, C. (2023). The JAK/STAT/NF-κB signaling pathway can be regulated by rosemary essential oil, thereby providing a potential treatment for DNCB-induced in mice. *Biomedicine & Pharmacotherapy, 168*, Article 115727. https://doi.org/10.1016/j.biopha.2023.115727

Li, L., Li, X., & Xie, K. (2012). GC-MS analysis of the essential oil composition of rosemary from Yuzhou, Henan, China. *Journal of Northwest Agriculture and Forestry University (Natural Science Edition), 40*(09). https://doi.org/10.13207/j.cnki.jnwafu.2012.09.007

Li, T., Han, X., Bao, R., Hao, Y., & Li, S. (2019). Preparation and properties of water-in-oil shiitake mushroom polysaccharide nanoemulsion. *International Journal of Biological Macromolecules, 140*, 343–349. https://doi.org/10.1016/j.ijbiomac.2019.08.134

Li, T., Wang, W., Guo, Q., Li, J., Tang, T., Wang, Y., Liu, D., Yang, K., Li, J., Deng, K., Wang, F., Li, H., Wu, Z., Guo, J., Guo, D., Shi, Y., Zou, J., Sun, J., Zhang, X., & Yang, M. (2024). Rosemary (Rosmarinus officinalis L.) hydrosol based on serotonergic synapse for insomnia. *Journal of Ethnopharmacology, 318*(Pt B), 116984. https://doi.org/10.1016/j.jep.2023.116984

Li, X., Liu, C., Liang, J., Zhou, L., Li, J., Chen, H., Jiang, T., Guan, Y., & Eng Khoo, H. (2022). Antioxidative mechanisms and anticolitic potential of Desmodium styracifolium (Osb.) Merr. in DSS-induced colitic mice. *Journal of Functional Foods, 93*, Article 105077. https://doi.org/10.1016/j.jff.2022.105077

Liang, Y., Zou, J., Zhang, X., Shi, Y., Tai, J., Wang, Y., Guo, D., & Yang, M. (2020). Preparation and quality evaluation of a volatile oil microemulsion from Flos magnoliae and Centipeda minima. *Molecular Medicine Reports, 22*(6), 4531–4540. https://doi.org/10.3892/mmr.2020.11571

Liu, C., Wang, R., Jiao, X., Zhang, J., Zhang, C., & Wang, Z. (2023). Oxysophocarpine suppresses TRAF6 level to ameliorate oxidative stress and inflammatory factors secretion in mice with dextran sulphate sodium (DSS) induced-ulcerative colitis. *Microbial Pathogenesis, 182*, Article 106244. https://doi.org/10.1016/j.micpath.2023.106244

Liu, C., Yin, Z., Feng, T., Zhang, M., Zhou, Z., & Zhou, Y. (2021a). An integrated network pharmacology and RNA-Seq approach for exploring the preventive effect of Lonicerae japonicae flos on LPS-induced acute lung injury. *Journal of Ethnopharmacology, 264*, Article 113364. https://doi.org/10.1016/j.jep.2020.113364

Liu, Q., Gao, Y., Fu, X., Chen, W., Yang, J., Chen, Z., Wang, Z., Zhuansun, X., Feng, J., & Chen, Y. (2021b). Preparation of peppermint oil nanoemulsions: Investigation of stability, antibacterial mechanism and apoptosis effects. *Colloids and Surfaces. B, Biointerfaces, 201*, Article 111626. https://doi.org/10.1016/j.colsurfb.2021.111626

Lu, L., Townsend, K. A., & Daigle, B. J., Jr. (2021). GEOlimma: Differential expression analysis and feature selection using pre-existing microarray data. *BMC Bioinformatics, 22*(1), 44. https://doi.org/10.1186/s12859-020-03932-5

Ma, C., Lin, W., Liu, Z., Tang, W., Gautam, R., Li, H., Qian, Y., Huang, H., & Wang, X. (2017). NDR1 protein kinase promotes IL-17- and TNF-α-mediated inflammation by competitively binding TRAF3. *EMBO Reports, 18*(4), 586–602. https://doi.org/10.15252/embr.201642140

Ma, J. S., Kim, W. J., Kim, J. J., Kim, T. J., Ye, S. K., Song, M. D., Kang, H., Kim, D. W., Moon, W. K., & Lee, K. H. (2010). Gold nanoparticles attenuate LPS-induced NO production through the inhibition of NF-kappaB and IFN-beta/STAT1 pathways in RAW264.7 cells. *Nitric Oxide, 23*(3), 214–219. https://doi.org/10.1016/j.niox.2010.06.005

Medicherla, K., Ketkar, A., Sahu, B. D., Sudhakar, G., & Sistla, R. (2016). Rosmarinus officinalis L. extract ameliorates intestinal inflammation through MAPKs/NF-κB signaling in a murine model of acute experimental colitis. *Food & Function, 7*(7), 3233–3243. https://doi.org/10.1039/c6fo00244g

Moghassemi, S., Dadashzadeh, A., Azevedo, R. B., & Amorim, C. A. (2022). Nanoemulsion applications in photodynamic therapy. *Journal of Controlled Release, 351*, 164–173. https://doi.org/10.1016/j.jconrel.2022.09.035

Noviello, D., Mager, R., Roda, G., Borroni, R. G., Fiorino, G., & Vetrano, S. (2021). The IL23-IL17 immune axis in the treatment of ulcerative colitis: Successes, defeats, and ongoing challenges. *Frontiers in Immunology, 12*, Article 611256. https://doi.org/10.3389/fimmu.2021.611256

Ordás, I., Eckmann, L., Talamini, M., Baumgart, D. C., & Sandborn, W. J. (2012). Ulcerative colitis. *Lancet, 380*(9853), 1606–1619. https://doi.org/10.1016/s0140-6736(12)60150-0

Park, M. Y., Ha, S. E., Kim, H. H., Bhosale, P. B., Abusaliya, A., Jeong, S. H., Park, J. S., Heo, J. D., & Kim, G. S. (2022). Scutellarein inhibits LPS-induced inflammation through NF-κB/MAPKs signaling pathway in RAW264.7 cells. *Molecules, 27*(12). https://doi.org/10.3390/molecules27123782

Pelvan, E., Karaoğlu, Ö., Önder Fırat, E., Betül Kalyon, K., Ros, E., & Alasalvar, C. (2022). Immunomodulatory effects of selected medicinal herbs and their essential oils: A comprehensive review. *Journal of Functional Foods, 94*, Article 105108. https://doi.org/10.1016/j.jff.2022.105108

Pinci, F., Gaidt, M. M., Jung, C., Kuut, G., Jackson, M. A., Bauernfried, S., & Hornung, V. (2020). C-tag TNF: A reporter system to study TNF shedding. *The Journal of Biological Chemistry, 295*(52), 18065–18075. https://doi.org/10.1074/jbc.RA120.015248

Romo Vaquero, M., Yáñez-Gascón, M. J., García Villalba, R., Larrosa, M., Fromentin, E., Ibarra, A., Roller, M., Tomás-Barberán, F., Espín de Gea, J. C., & García-Conesa, M. T. (2012). Inhibition of gastric lipase as a mechanism for body weight and plasma lipids reduction in Zucker rats fed a rosemary extract rich in carnosic acid. *PLoS One, 7*(6), e39773. https://doi.org/10.1371/journal.pone.0039773

Rose-John, S. (2012). IL-6 trans-signaling via the soluble IL-6 receptor: Importance for the pro-inflammatory activities of IL-6. *International Journal of Biological Sciences, 8*(9), 1237–1247. https://doi.org/10.7150/ijbs.4989

Sari, T. P., Mann, B., Kumar, R., Singh, R. R. B., Sharma, R., Bhardwaj, M., & Athira, S. (2015). Preparation and characterization of nanoemulsion encapsulating curcumin. *Food Hydrocolloids, 43*, 540–546. https://doi.org/10.1016/j.foodhyd.2014.07.011

Seok, S. H., Lee, S.-A., & Park, E.-S. (2018). Formulation of a microemulsion-based hydrogel containing celecoxib. *Journal of Drug Delivery Science and Technology, 43*, 409–414. https://doi.org/10.1016/j.jddst.2017.11.016

Shalaby, M., Abdelaziz, R. R., Ghoneim, H. A., & Suddek, G. M. (2023). Imatinib mitigates experimentally-induced ulcerative colitis: Possible contribution of NF-kB/JAK2/STAT3/COX2 signaling pathway. *Life Sciences, 321*, Article 121596. https://doi.org/10.1016/j.lfs.2023.121596

Shi, W., Yan, R., & Huang, L. (2022). Preparation and insecticidal performance of sustained-release cinnamon essential oil microemulsion. *Journal of the Science of Food and Agriculture, 102*(4), 1397–1404. https://doi.org/10.1002/jsfa.11472

Swaidani, S., Liu, C., Zhao, J., Bulek, K., & Li, X. (2019). TRAF regulation of IL-17 cytokine signaling. *Frontiers in Immunology, 10*, 1293. https://doi.org/10.3389/fimmu.2019.01293

Takaki, I., Bersani-Amado, L. E., Vendruscolo, A., Sartoretto, S. M., Diniz, S. P., Bersani-Amado, C. A., & Cuman, R. K. (2008). Anti-inflammatory and antinociceptive effects of Rosmarinus officinalis L. essential oil in experimental animal models. *Journal of Medicinal Food, 11*(4), 741–746. https://doi.org/10.1089/jmf.2007.0524

Tanaka, T., & Kishimoto, T. (2012). Immunotherapeutic implication of IL-6 blockade. *Immunotherapy, 4*(1), 87–105. https://doi.org/10.2217/imt.11.147

Vitória Minzoni de Souza Iacia, M., Eduarda Ferraz Mendes, M., Cristiny de Oliveira Vieira, K., Cristine Marques Ruiz, G., José Leopoldo Constantino, C., da Silva Martin, C., Eloizo Job, A., Alborghetti Nai, G., & Kretli Winkelstroter Eller, L. (2024). Evaluation of curcumin nanoemulsion effect to prevent intestinal damage. *International Journal of Pharmaceutics, 650*, Article 123683. https://doi.org/10.1016/j.ijpharm.2023.123683

Wang, H., Pan, F., Liu, J., Zhang, J., Fuli, Z., & Wang, Y. (2024a). Huayuwendan decoction ameliorates inflammation via IL-17/NF-κB signaling pathway in diabetic rats. *Journal of Ethnopharmacology, 319*(Pt 3), Article 117328. https://doi.org/10.1016/j.jep.2023.117328

Wang, J., Zhang, Q., Deng, Y., Deng, G., Huang, F., Zhou, Y., Jia, M., & Yi, H. (2021a). Efficacy and safety of heat-sensitive moxibustion in the treatment of ulcerative colitis: A protocol for a systematic review and meta-analysis. *Medicine (Baltimore), 100*(4), e24078. https://doi.org/10.1097/md.0000000000024078

Wang, W., Wang, Y., Zou, J., Jia, Y., Wang, Y., Li, J., Wang, C., Sun, J., Guo, D., Wang, F., Wu, Z., Yang, M., Wu, L., Zhang, X., & Shi, Y. (2021b). The mechanism action of german chamomile (Matricaria recutita L.) in the treatment of eczema: based on dose-effect weight coefficient network pharmacology. *Frontiers in Pharmacology., 12*, 706836. https://doi.org/10.3389/fphar.2021.706836

Wang, X., Zhou, P., Shi, H., Wang, W., Li, T., Tang, T., Duan, J., Li, J., Xia, N., Wang, J., Chen, C., Wang, J., Zou, J., Shi, Y., Guo, D., Wu, Z., Yang, M., Zhang, X., & Sun, J. (2023). Cinnamon essential oil based on NLRP3 inflammasome and renal uric acid transporters for hyperuricemia. *Food Bioscience, 56*, Article 103285. https://doi.org/10.1016/j.fbio.2023.103285

Wang, Y., Wang, X., Tang, T., Xie, Y., Li, J., Wang, W., Li, T., Liu, D., Yang, K., Shi, Y., Sun, J., Guo, D., Zou, J., Bai, F., Sun, Y., Zhang, X., & Wang, C. (2024b). Basis with RNA-Seq and WGCNA to explore the effect of Frankincense essential oil on dextran sodium sulfate-induced ulcerative colitis through MAPK/NF-κB signaling. *Fitoterapia, 172*, Article 105744. https://doi.org/10.1016/j.fitote.2023.105744

Wang, Y., Zou, J., Jia, Y., Zhang, X., Wang, C., Shi, Y., Guo, D., Wu, Z., & Wang, F. (2021c). The mechanism of lavender essential oil in the treatment of acute colitis based on "quantity-effect" weight coefficient network pharmacology. *Frontiers in Pharmacology, 12*, Article 644140. https://doi.org/10.3389/fphar.2021.644140

Wei, F., Zhang, Y., Jian, J., Mundra, J. J., Tian, Q., Lin, J., Lafaille, J. J., Tang, W., Zhao, W., Yu, X., & Liu, C. J. (2014). PGRN protects against colitis progression in mice in an IL-10 and TNFR2 dependent manner. *Scientific Reports, 4*, 7023. https://doi.org/10.1038/srep07023

Wei, L., Liu, M., Xiong, H., & Peng, B. (2018). Up-regulation of IL-23 expression in human dental pulp fibroblasts by IL-17 via activation of the NF-κB and MAPK pathways. *International Endodontic Journal, 51*(6), 622–631. https://doi.org/10.1111/iej.12871

Wu, B. (2022). Acute moderate to severe ulcerative colitis treated by traditional Chinese medicine: A case report. *World Journal of Clinical Cases, 10*(36), 13356–13363. https://doi.org/10.12998/wjcc.v10.i36.13356

Wu, L., Wang, C., Boisson, B., Misra, S., Rayman, P., Finke, J. H., Puel, A., Casanova, J. L., & Li, X. (2014). The differential regulation of human ACT1 isoforms by Hsp90 in IL-17 signaling. *Journal of Immunology, 193*(4), 1590–1599. https://doi.org/10.4049/jimmunol.1400715

Xiang, P., Chen, T., Mou, Y., Wu, H., Xie, P., Lu, G., Gong, X., Hu, Q., Zhang, Y., & Ji, H. (2015). NZ suppresses TLR4/NF-κB signalings and NLRP3 inflammasome activation in LPS-induced RAW264.7 macrophages. *Inflammation Research, 64*(10), 799–808. https://doi.org/10.1007/s00011-015-0863-4

Yan, W. F., Gao, X. H., Yang, R. X., Zhao, X. W., Luo, H., Li, Z., & Yang, H. (2022). Response surface methodology for optimizing the extraction of rosemary essential oil by atmospheric distillation. *Chinese seasonings, 47*(11), 115–119.

Yin, H., Liu, W., Ji, X., Yan, G., Zeng, X., Zhao, W., & Wang, Y. (2023). Study on the mechanism of Wumei San in treating piglet diarrhea using network pharmacology and molecular docking. *Front Vet Sci, 10*, 1138684. https://doi.org/10.3389/fvets.2023.1138684

Yan, Q., Xue, Y., Li, F., Wang, F., Qin, Z., Dai, B., & Yuan, H. (2023). Preparation and in vitro evaluation of a novel ionic liquid microemulsion of glycyrrhizic acid. *Chinese herbal medicine, 54*(01), 62–71.

Zeng, Z., Zhou, G., Wang, X., Huang, E. Z., Zhan, X., Liu, J., Wang, S., Wang, A., Li, H., Pei, X., & Xie, T. (2010). Preparation, characterization and relative bioavailability of oral elemene o/w microemulsion. *International Journal of Nanomedicine, 5*, 567–572. https://doi.org/10.2147/ijn.s12485

Zhang, C., Luo, G., Lin, J., Zhao, Z., Luo, M., & Li, H. (2022a). Identification of significant modules and hub genes involved in hepatic encephalopathy using WGCNA. *European Journal of Medical Research, 27*(1), 264. https://doi.org/10.1186/s40001-022-00898-3

Zhang, H., Guo, Z., Wang, X., Xian, J., Zou, L., Zheng, C., & Zhang, J. (2022b). Protective mechanisms of Zanthoxylum bungeanum essential oil on DSS-induced ulcerative colitis in mice based on a colonic mucosal transcriptomic approach. *Food & Function, 13*(18), 9324–9339. https://doi.org/10.1039/d1fo04323d

Zhang, J., & Shi, G. (2020). Lymphocyte infiltration and key differentially expressed genes in the ulcerative colitis. *Medicine (Baltimore), 99*(35), e21997. https://doi.org/10.1097/md.0000000000021997

Zhou, G., Kong, W. S., Li, Z. C., Xie, R. F., Yu, T. Y., & Zhou, X. (2021). Effects of qing chang suppository powder and its ingredients on IL-17 signal pathway in HT-29 cells and DSS-induced mice. *Phytomedicine, 87*, Article 153573. https://doi.org/10.1016/j.phymed.2021.153573

Zhu, F., Ke, Y., Luo, Y., Wu, J., Wu, P., Ma, F., & Liu, Y. (2021). Effects of different treatment of fecal microbiota transplantation techniques on treatment of ulcerative colitis in rats. *Frontiers in Microbiology, 12*, Article 683234. https://doi.org/10.3389/fmicb.2021.683234